

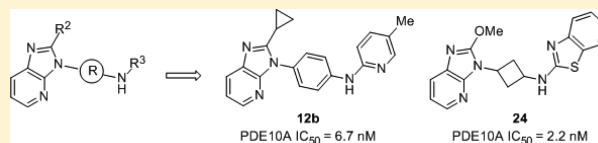
Discovery of Novel Imidazo[4,5-*b*]pyridines as Potent and Selective Inhibitors of Phosphodiesterase 10A (PDE10A)Essa Hu,<sup>\*,†</sup> Kristin Andrews,<sup>‡</sup> Samer Chmait,<sup>‡</sup> Xiaoning Zhao,<sup>‡</sup> Carl Davis,<sup>§</sup> Silke Miller,<sup>||</sup> Geraldine Hill Della Puppa,<sup>||</sup> Mary Dovlatyan,<sup>||</sup> Hang Chen,<sup>∇</sup> Dianna Lester-Zeiner,<sup>∇</sup> Jessica Able,<sup>∇</sup> Christopher Biorn,<sup>∇</sup> Ji Ma,<sup>○</sup> Jianxia Shi,<sup>○</sup> James Treanor,<sup>||</sup> and Jennifer R. Allen<sup>†</sup>

<sup>†</sup>Department of Medicinal Chemistry, <sup>‡</sup>Department of Molecular Structure, <sup>§</sup>Department of Pharmacokinetics and Drug Metabolism, and <sup>||</sup>Department of Neuroscience, Amgen, Inc., One Amgen Center Drive, Thousand Oaks, California 93012-1799, United States  
<sup>∇</sup>Department of Molecular Structure and Characterization, <sup>∇</sup>Department of Neuroscience, and <sup>○</sup>Department of Pharmacokinetics and Drug Metabolism, Amgen, Inc., 1120 Veterans Boulevard, South San Francisco, California 94080, United States

## Supporting Information

**ABSTRACT:** We report the discovery of novel imidazo[4,5-*b*]pyridines as potent and selective inhibitors of PDE10A. The investigation began with our recently disclosed ketobenzimidazole **1**, which exhibited single digit nanomolar PDE10A activity but poor oral bioavailability. To improve oral bioavailability, we turned to novel scaffold imidazo[4,5-*b*]pyridine **2**, which not only retained nanomolar PDE10A activity but was also devoid of the morpholine metabolic liability. Structure–activity relationship studies were conducted systematically to examine how various regions of the molecule impacted potency. X-ray cocrystal structures of compounds **7** and **24** in human PDE10A helped to elucidate the key bonding interactions. Five of the most potent and structurally diverse imidazo[4,5-*b*]pyridines (**4**, **7**, **12b**, **24a**, and **24b**) with PDE10A IC<sub>50</sub> values ranging from 0.8 to 6.7 nM were advanced into receptor occupancy studies. Four of them (**4**, **12b**, **24a**, and **24b**) achieved 55–74% RO at 10 mg/kg po.

**KEYWORDS:** Phosphodiesterase 10A, schizophrenia, receptor occupancy, bioavailability



Phosphodiesterase (PDE) enzymes regulate the intracellular signaling of cyclic adenosine 3'-5'-monophosphate (cAMP) and cyclic guanosine 3'-5'-monophosphate (cGMP) by cleaving their phosphodiester bonds and converting them to AMP and GMP. The PDE isoforms are highly localized, positioned to modulate the cNMP gradients and signaling in a specific tissue. Since 10 out of 11 PDE isoforms have splice variants in the CNS, it has been postulated that having a means to control the activity of a specific PDE isoform in the CNS could be beneficial to a range of neuropsychiatric and neurodegenerative diseases such as psychosis, depression, Parkinson's disease, Alzheimer's disease, etc.<sup>1–3</sup>

An in depth analysis of the medications prescribed for treatment of schizophrenia revealed a disease area with significant unmet medical needs.<sup>4</sup> The current standard of care (SOC) was found to be inadequate, with limited efficacy and adverse effects on patient quality of life. Since these SOC shared similar mechanisms of action, the authors concluded that novel targets should be explored for future drug development. PDE10A represented such a novel target opportunity for treatment of schizophrenia.<sup>5</sup> The PDE10A enzyme is highly expressed in the striatum, a brain region believed to be dysregulated in schizophrenia. In a locomotor behavioral model, PDE10A knockout mice showed blunted response when treated with PCP suggesting that a PDE10A antagonist could have therapeutic benefit.<sup>6</sup> Since PDE10A is positioned to modulate levels of cAMP and cGMP downstream

of dopaminergic pathways and glutamatergic pathways, two major pathways that have been associated with the pathophysiology of schizophrenia, it has been hypothesized that inhibition of PDE10A could be used to treat all three main symptoms of schizophrenia, the positive, the negative, and the cognitive deficits.<sup>7</sup> To date, at least two PDE10A inhibitors have been advanced into clinical trials to test this hypothesis.<sup>8</sup>

We recently reported the discovery of ketobenzimidazole **1** as an inhibitor of PDE10A (Figure 1).<sup>9</sup> This compound exhibited single digit nanomolar activity against PDE10A enzyme (IC<sub>50</sub> = 4.5 nM) with moderate in vivo clearance in

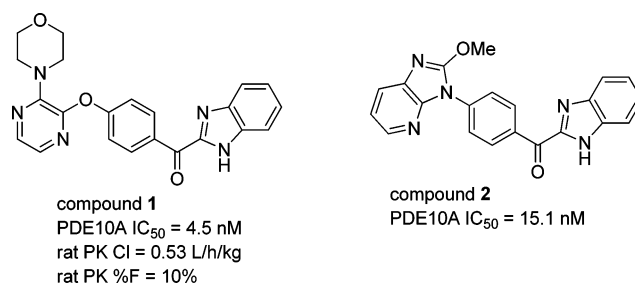


Figure 1. Structures of compounds **1** and **2**.

Received: March 7, 2014

Accepted: March 28, 2014

Published: March 28, 2014

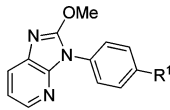
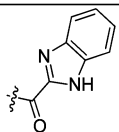
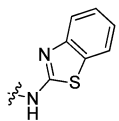
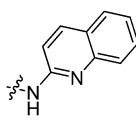
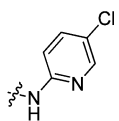
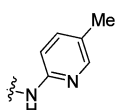
rat (Cl = 0.53 L/h/kg). However, its oral bioavailability was low (10% F). Poor permeability and metabolic instability have been found to be two common causes of poor oral bioavailability.<sup>10</sup> Since **1** was highly permeable, we focused our efforts on reducing its metabolic liability. As disclosed in our recent report, we found that replacement of the morpholine ring with metabolically robust heterocycles improved its pharmacokinetic (PK) profile.<sup>9</sup> Meanwhile, we searched for a novel scaffold devoid of a morpholine to circumvent the PK issue. One intriguing lead that emerged from this search was imidazo[4,5-*b*]pyridine **2**, which exhibited comparable PDE10A inhibitory activity (IC<sub>50</sub> = 15.1 nM) to **1**. In this letter, we present our thorough examination of the structure–activity relationship (SAR) of this novel scaffold and our discovery of structurally diverse, potent, and selective inhibitors of PDE10A with improved in vivo profiles.

We began with an investigation of linker and benzimidazole replacements (Table 1). As we had observed with ketobenzimidazole **1**, replacement of the carbonyl linker with an amine (**3**) resulted in a 30-fold boost in potency but a high P-gp efflux ratio. Amino benzthiazole **4** not only showed a 3-fold increase in potency (IC<sub>50</sub> = 5.7 nM) compared to **2** but also maintained a low efflux ratio in P-gp assays (1.6 in human; 1.7 in rat) and acceptable in vitro clearance (65 μL/min/mg in human; 62 μL/min/mg in rat). Significant erosion of PDE10A potency was observed with quinoline **5** suggesting the 6–6 fused system may be too bulky for the binding pocket. Interestingly, while chloro pyridine **6** experienced a reduction of PDE10A activity, methylpyridine **7** (IC<sub>50</sub> = 4.1 nM) was 10-fold more potent than **6**. Analogue **7** also exhibited low in vitro clearance (34 μL/min/mg in human; 27 μL/min/mg in rat) plus low P-gp efflux ratios (1.4 in human; 1.9 in rat).

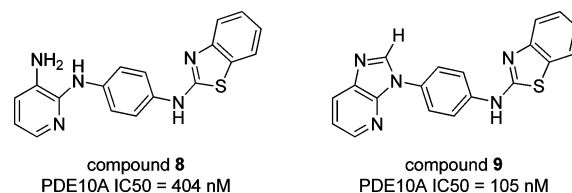
As shown in Figure 2, the methoxy imidazo[4,5-*b*]pyridine motif was also found to be necessary for PDE10A inhibitory activity. Opening the imidazole ring (**8**) greatly deteriorated the potency of the compound. Removal of the methoxy substituent (**9**) also afforded a much weaker analogue compared to **4**. To understand how the methoxy substituent helped to increase PDE10A binding affinity, we embarked on a systematic examination of the methoxy substituent on benzthiazole **4** and pyridine **7** (Table 2). Replacement with a methyl group (**10a** and **10b**) decreased potency compared to their methoxy analogues **4** and **7**. Extending the substitution to an ethyl group (**11a** and **11b**) had minimal impact on activity, indicating the electron withdrawing oxygen atom on the methoxy substituent had a critical role in the potency of the compounds. To our surprise, while cyclopropyl benzthiazole **12a** showed no change in potency from its ethyl analogue **11a**, cyclopropyl methylpyridine **12b** achieved single digit nanomolar potency (IC<sub>50</sub> = 6.7 nM), 7-fold more potent than its ethyl analogue **11b**.

General synthetic routes for compounds **2**–**12b** are shown in Scheme 1. Route A illustrated the synthesis of compound **2**, which began with protection of benzimidazole **13** and deprotonation using LHMDS to add to methyl 4-iodobenzoate **14** to afford ketobenzimidazole intermediate **15**. Palladium catalyzed coupling of 3-nitropyridin-2-amine **16** followed by nitro reduction using molybdenum hexacarbonyl produced (4-((3-aminopyridin-2-yl)amino)phenyl)(1-(tetrahydro-2H-pyran-2-yl)-1H-benzo[*d*]imidazol-2-yl)methanone **17**. Acid promoted synthesis of imidazo[4,5-*b*]pyridine core and sulfuric acid deprotection of THP group formed (1H-benzo[*d*]imidazol-2-yl)(4-(2-methoxy-3H-imidazo[4,5-*b*]pyridin-3-yl)-

**Table 1. Examination of Linker and Benzimidazole Replacements on Compound 2**

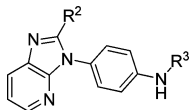
Cmpd	R <sup>1</sup>	PDE10A	LM	Efflux
		IC <sub>50</sub> (nM) <sup>a</sup>	(μL/min/mg) <sup>b</sup>	Ratio <sup>c</sup>
<b>2</b>		15.1 ± 0.5	56 (h)	1.2 (h)
			22 (r)	1.1 (r)
<b>3</b>		0.5 ± 0.2	24 (h)	7.2 (h)
			58 (r)	12.8 (r)
<b>4</b>		5.7 ± 1.9	65 (h)	1.6 (h)
			62 (r)	1.7 (r)
<b>5</b>		115 ± 2.1	57 (h)	NT
			97 (r)	NT
<b>6</b>		39.8 ± 3.4	32 (h)	NT
			70 (r)	NT
<b>7</b>		4.1 ± 1.5	34 (h)	1.4 (h)
			27 (r)	1.9 (r)

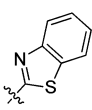
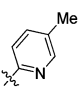
<sup>a</sup>Each IC<sub>50</sub> value reported was an average of at least two independent experiments with 22 point dose–response curve in duplicates at each concentration. <sup>b</sup>In vitro human and rat liver microsomal stability studies were conducted in the presence of NADPH at 37 °C for 30 min at a final compound concentration of 1 μM of compound. <sup>c</sup>Human and rat efflux ratio reported was based on the ratio of the basolateral to apical permeability over apical to basolateral permeability of a compound. MDCK-Madin-Darby canine kidney (MDCK) cells were used to measure the compound's apparent permeability in each direction. (h): human. (r): rat. LM: liver microsomal stability. NT: not tested.



**Figure 2.** Structures of compounds **8** and **9**.

phenyl)methanone **2**. Route B depicted the general synthetic scheme for analogues **3**–**12b**. Coupling of *N*-(4-aminophenyl)-acetamide **18** with 2-chloro-3-nitropyridine **19** by S<sub>N</sub>Ar

**Table 2. Examination of Methoxy Replacements on Compounds 4 and 7**


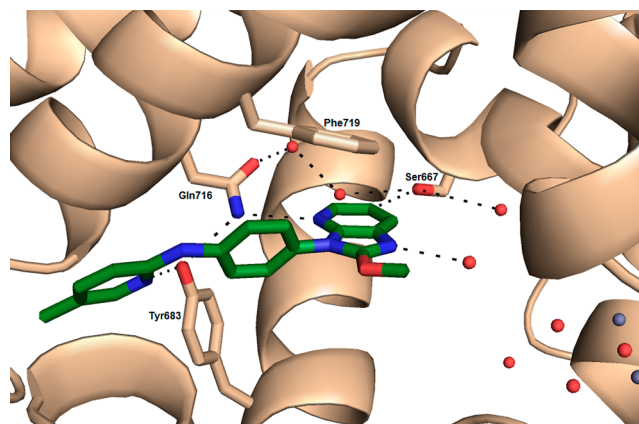
Cmpd	R <sup>2</sup>	PDE10A IC <sub>50</sub> (nM) <sup>a</sup>	
		R <sup>3</sup> = 	R <sup>3</sup> = 
<b>4</b>	-OMe	5.7 ± 1.9	
<b>7</b>	-OMe		4.1 ± 1.5
<b>10a</b>	-Me	36.8 ± 0.6	
<b>10b</b>	-Me		51.5 ± 0.6
<b>11a</b>	-Et	21.5 ± 0.6	
<b>11b</b>	-Et		47.3 ± 0.2
<b>12a</b>	-cPr	20.7 ± 0.4	
<b>12b</b>	-cPr		6.7 ± 1.0

<sup>a</sup>Each IC<sub>50</sub> value reported was an average of at least two independent experiments with 22 point dose–response curve in duplicates at each concentration.

displacement reaction followed by removal of acetyl protecting group gave *N*-(3-nitro-pyridin-2-yl)-benzene-1,4-diamine (**20**). A second S<sub>N</sub>Ar displacement to install the desired R<sup>3</sup> ring followed by reduction of the nitro group using palladium hydrogenation afforded aniline intermediate **21**. Finally, acid

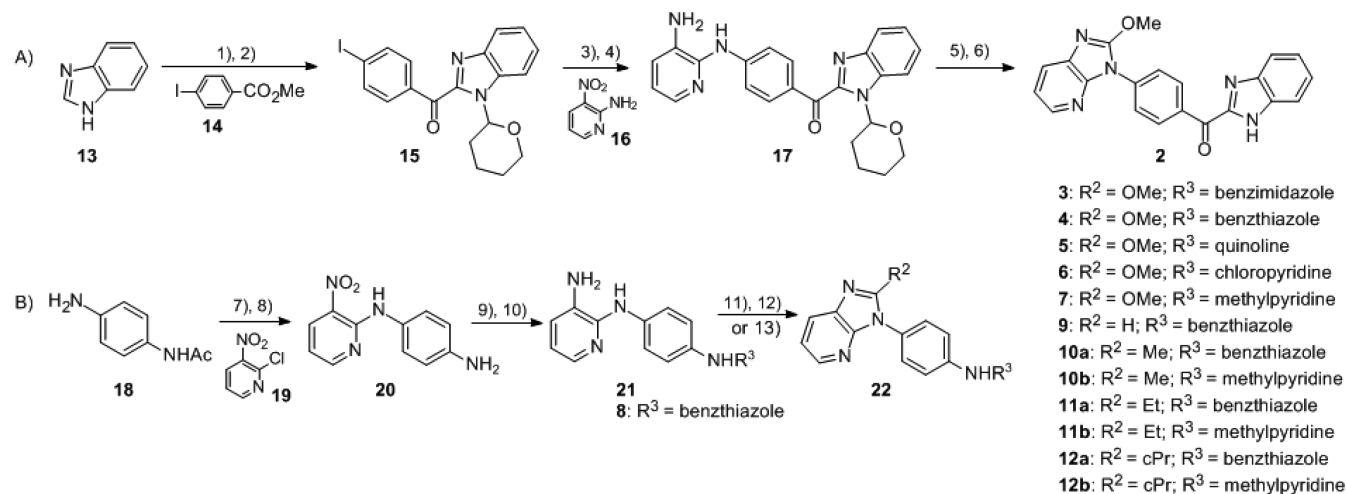
catalyzed cyclization formed the desired imidazo[4,5-*b*]pyridine **22**.

We were able to obtain an X-ray cocrystal structure of imidazo[4,5-*b*]pyridine **7** in the human PDE10A catalytic binding domain in order to elucidate the key binding interactions of this novel scaffold (Figure 3). Two critical

**Figure 3.** X-ray cocrystal structure of compound **7** in human PDE10A enzyme.

hydrogen bonding interactions were observed. The first interaction was between the pyridine nitrogen on imidazo[4,5-*b*]pyridine and the conserved Gln716. The other interaction was between the pyridine nitrogen on the methylpyridine and Tyr683. The center phenyl ring did not appear to be making any binding interactions with the PDE10A enzyme. Instead, it served as a scaffold that enabled both imidazo[4,5-*b*]pyridine and methylpyridine rings to make the critical hydrogen binding interactions with the PDE10A enzyme.

To further explore the role of the middle phenyl ring, we examined other moieties that could still maintain the linear orientation between the imidazo[4,5-*b*]pyridine and the

**Scheme 1. Syntheses of Compounds 2–12b<sup>a</sup>**

<sup>a</sup>Reagents and conditions: (1) 3,4-dihydro-2*H*-pyran, *p*-toluenesulfonic acid, 130 °C, 88% yield; (2) **14**, LHMDS, THF, –78 °C, 33% yield; (3) Pd<sub>2</sub>(dba)<sub>3</sub>, Xantphos, **16**, Cs<sub>2</sub>CO<sub>3</sub>, DMA, 100 °C, 98% yield; (4) Mo(CO)<sub>6</sub>, DBU, EtOH, 150 °C, 77% yield; (5) propionic acid, tetramethyl orthoformate, 100 °C, 50% yield; (6) sulfuric acid, THF, EtOAc, –20 °C, 23% yield; (7) **19**, TEA, DMSO, 90 °C, 90% yield; (8) 5 N HCl, 1,4-dioxane, 70 °C, 90% yield; (9) 2-chloro-5-methyl-pyridine, 180 °C; (10) Pd/C, MeOH, H<sub>2</sub>; (11) propionic acid, HATU, TEA, DCM, room temperature; (12) acetic acid, 90 °C; (13) tetramethyl orthoformate, propionic acid, 90 °C.

methylpyridine (Table 3). With a cyclohexyl group as the central ring, **23** experienced a significant reduction in potency.

**Table 3. Examination of Central Phenyl Ring Replacements**

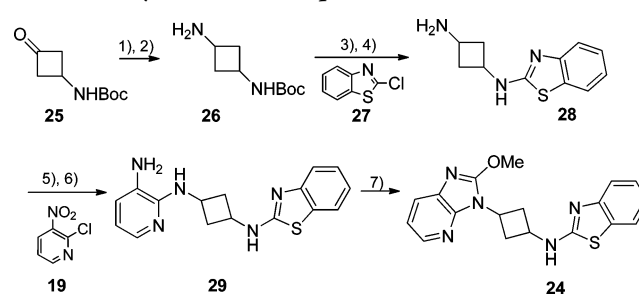
Cmpd	Structure	PDE10A IC <sub>50</sub> (nM) <sup>a</sup>	LM (μL/min/mg) <sup>b</sup>
<b>4</b>		5.7 ± 1.9	65 (h) 62 (r)
<b>23</b>		271 ± 29.7	101 (h) 367 (r)
<b>24</b>		2.2 ± 0.1	
<b>24a</b>		3.4 ± 1.4	80 (h) 199 (r)
<b>24b</b>		0.8 ± 0.3	82 (h) 152 (r)

<sup>a</sup>Each IC<sub>50</sub> value reported was an average of at least two independent experiments with 22 point dose–response curve in duplicates at each concentration. <sup>b</sup>In vitro human and rat liver microsomal stability studies were conducted in the presence of NADPH at 37 °C for 30 min at a final compound concentration of 1 μM of compound. (h): human. (r): rat. LM: liver microsomal stability.

Presumably, the cyclohexyl ring was too bulky to fit in the narrow channel between Gln716 and Tyr683. To our surprise, *cis/trans*-cyclobutyl mixture **24** exhibited single digit nanomolar activity (IC<sub>50</sub> = 2.2 nM) comparable to its phenyl analogue **4**. We separated the mixtures and found the *cis*-cyclobutyl isomer (**24a**) had an IC<sub>50</sub> of 3.4 nM against PDE10A and the *trans*-cyclobutyl isomer (**24b**) had an IC<sub>50</sub> of 0.8 nM against PDE10A.

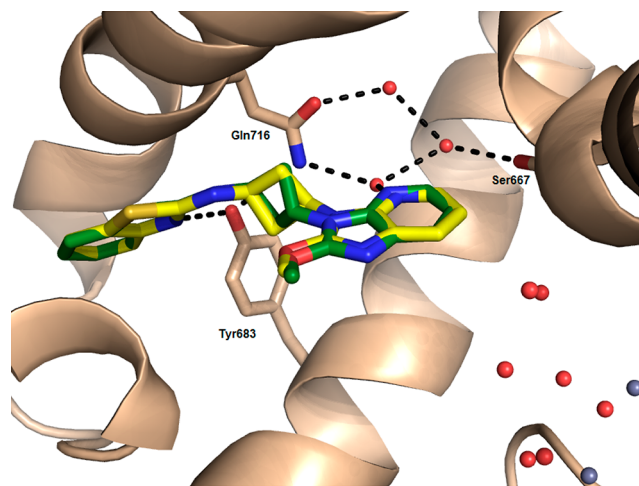
The synthesis of compound **24** was accomplished as depicted in Scheme 2. Reductive amination of *tert*-butyl (3-oxocyclobutyl)carbamate **25** with benzylamine followed by deprotective hydrogenation afforded *tert*-butyl (3-aminocyclobutyl)carbamate **26** as mixture of *cis* and *trans* isomers. Installation of benzthiazole ring via S<sub>N</sub>Ar displacement using chlorobenzthiazole **27** then acid catalyzed removal of Boc protecting group gave N<sup>1</sup>-(benzo[*d*]thiazol-2-yl)cyclobutane-1,3-diamine **28**. Installation of 3-aminopyridine via first S<sub>N</sub>Ar displacement with 2-chloro-3-nitropyridine **19** then nitro reduction by hydrogenation afforded N<sup>2</sup>-(3-(benzo[*d*]thiazol-2-ylamino)cyclobutyl)pyridine-2,3-diamine **29**. Acid promoted cyclization formed the *cis/trans*-imidazo[4,5-*b*]pyridine **24**. Separation by chiral chromatography led to the isolation of *cis*-cyclobutyl isomer **24a** and *trans*-cyclobutyl isomer **24b**.

**Scheme 2. Synthesis of Compound 24<sup>a</sup>**



<sup>a</sup>Reagents and conditions: (1) benzylamine, sodium cyanoborohydride, MeOH, 80% yield; (2) 50% Pd(OH)<sub>2</sub>/C, MeOH, H<sub>2</sub>, 95% yield; (3) **27**, DIPEA, NMP, 180 °C, 50% yield; (4) HCl, MeOH; (5) **19**, sodium carbonate, DMF, reflux, 70% yield for two steps; (6) 50% Pd/C, MeOH, H<sub>2</sub>, 97% yield; (7) propionic acid, tetramethyl orthocarbonate, 90 °C, 63% yield.

We were able to obtain an X-ray cocrystal structure of *cis/trans* mixture **24** in the human PDE10A catalytic domain (Figure 4). An overlap of both isomers (*cis* isomer colored



**Figure 4.** Overlap of X-ray cocrystal structure of *cis/trans* mixture **24** in human PDE10A enzyme. *Cis* isomer colored yellow. *Trans* isomer colored green.

yellow and *trans* isomers colored green) illustrated their nearly identical binding modes. Compared to cocrystal structure of compound **7** in PDE10A, the benzthiazole portion of both isomers maintained similar key hydrogen bond interactions with Tyr683. An extra water molecule was observed between the pyridine nitrogen on the imidazo[4,5-*b*]pyridine core and the conserved Gln716. Since both *cis* and *trans* cyclobutane rings were able to fit in the narrow channel between Gln716 and Tyr683, both *cis* isomer **24a** and *trans* isomer **24b** were able to achieve single digit nanomolar activity against PDE10A.

For the primary pharmacodynamic (PD) model, we were reluctant to use the prevalent rodent behavioral models since they could not discern whether the desired outcome was achieved as a result of on-target or off-target mechanism. We wanted a more direct and definitive readout of target engagement and chose instead to measure receptor occupancy (RO) as our PD readout. We recently disclosed the development of PDE10A tracer AMG7980 that provided a direct, in vivo measurement of PDE10A inhibition.<sup>11</sup> To determine whether the imidazo[4,5-*b*]pyridines could pass the

blood–brain barrier (BBB) and block the PDE10A enzymes in the CNS, all five single digit nanomolar imidazo[4,5-*b*]pyridine inhibitors (**4**, **7**, **12b**, **24a**, and **24b**) were dosed into Sprague–Dawley rats at 10 mg/kg po. The brains of the rodents were collected 1 h postdosing, and the level of CNS blockage was assessed by incubating brain slices with [<sup>3</sup>H]-AMG7980. As shown in Table 4, four compounds (**4**, **12b**, **24a**, and **24b**)

**Table 4.** PDE10A ex Vivo Receptor Occupancy<sup>a</sup> and in Vivo Rat PK<sup>b</sup> of Compounds **4**, **7**, **12b**, **24a**, and **24b**

compd	receptor occupancy	Cl (L/h/kg)	Auc (μM·h)	T <sub>1/2</sub> (h)	% F
<b>4</b>	55%	0.65	11.9	3.24	30
<b>7</b>	36%	1.17	7.56	3.78	28
<b>12b</b>	67%	2.05	3.44	0.91	24
<b>24a</b>	68%	0.88	10.7	2.1	32.5
<b>24b</b>	74%	0.21	16.0	3.5	7

<sup>a</sup>In vivo receptor occupancy measurements were taken 1 h post dosing of compounds at 10 mg/kg. <sup>b</sup>In vivo RO and PK studies were conducted in male Sprague–Dawley rats. Vehicles used: 100% DMSO for iv; 1% Tween, 2% HPMC with methanesulfonic acid, pH 2.2 for po.

achieved greater than 50% PDE10A occupancy in the ex vivo RO assay. Even though benzthiazole **4** and methylpyridine **7** exhibited similar PDE10A potency in the in vitro assay, compound **7** was only able to reach 36.4% occupancy compared to 54.5% of compound **4**, presumably due to the higher in vivo clearance of **7**. In contrast, compound **12b** was able to achieve 67% receptor occupancy despite its high in vivo clearance. We were excited to see both *cis* and *trans* isomers of cyclobutyl imidazo[4,5-*b*]pyridines (**24a** and **24b**) achieved excellent PDE10A RO (68% and 74%, respectively). Interestingly, these two isomers exhibited different in vivo PK profiles in rat: *cis*-cyclobutyl isomer **24a** showed modest clearance (Cl = 0.88 L/h/kg) and acceptable oral bioavailability (32.5% F), while *trans*-cyclobutyl isomer **24b** exhibited low clearance (Cl = 0.21 L/h/kg) but poor oral bioavailability (7% F).

To compare the in vivo efficacies of ketobenzimidazole **1** and these novel imidazo[4,5-*b*]pyridines, we advanced imidazo[4,5-*b*]pyridines **4** and **12b** to an LC–MS/MS RO assay, an in vivo RO measurement platform we had previously developed.<sup>11</sup> In this study, both the inhibitor and our PDE10A tracer AMG7980 were dosed in vivo, and then the relative levels of the compounds in the rat brain were quantified by LC–MS/MS. We had previously reported that ketobenzimidazole **1** produced 21% RO at 10 mg/kg po in the LC–MS/MS RO assay.<sup>9</sup> In contrast, at the same 10 mg/kg po dose, imidazo[4,5-*b*]pyridines **4** and **12b** achieved 71% RO and 57% RO, respectively, suggesting that these imidazo[4,5-*b*]pyridines were more efficacious than **1** in vivo.

We discovered a novel imidazo[4,5-*b*]pyridines core that resulted in the identification of several structurally diverse and potent inhibitors of PDE10A. Compared to ketobenzimidazole **1**, this new core was able to produce potent PDE10A activity without the metabolically labile morpholine. Both the methoxy substituent and the imidazole ring on the imidazo[4,5-*b*]pyridines core were critical for the binding affinity. To improve potency, the rigid carbonyl linker on ketobenzimidazole **2** was replaced with a more flexible amino linker. To maintain the low efflux ratio, the benzimidazole portion was replaced with either a benzthiazole (**4**) or a methylpyridine (**7**). Based on our analysis of the X-ray cocrystal structure of **7** in

PDE10A enzyme, we were able to replace the middle phenyl ring with cyclobutanes and obtained comparable or greater potency with either *cis*-cyclobutane **24a** (IC<sub>50</sub> = 3.4 nM) or *trans*-cyclobutane **24b** (IC<sub>50</sub> = 0.8 nM). Four imidazo[4,5-*b*]pyridines (**4**, **12b**, **24a**, and **24b**) achieved 55–74% RO at 10 mg/kg po in our PDE10A ex vivo RO study. Compounds **4** and **12b** also achieved 71% and 57% RO in the in vivo LC–MS/MS RO assay, reaching levels superior to the 21% RO shown by ketobenzimidazole **1**. All of the compounds advanced into the RO assay also exhibited greater than 30 μM activity against other PDE isoforms. An exhaustive SAR study of the cyclobutane series and their improved in vivo PK and efficacies will be reported in a separate publication.

## ■ ASSOCIATED CONTENT

### Supporting Information

Experimental procedures and analytical data, along with protocols for X-ray cocrystallization and biological assays. This material is available free of charge via the Internet at <http://pubs.acs.org>.

### Accession Codes

The PDB ID codes for coordinates of **7** and **24** with PDE10A are 4P1R and 4P0N, respectively.

## ■ AUTHOR INFORMATION

### Corresponding Author

\*(E.H.) Phone: 805-313-5300. E-mail: [ehu@amgen.com](mailto:ehu@amgen.com).

### Notes

The authors declare no competing financial interest.

## ■ ABBREVIATIONS

BBB, blood–brain barrier; cAMP, cyclic adenosine 3′-5′-monophosphate; cGMP, cyclic guanosine 3′-5′-monophosphate; ER, efflux ratio; HPMC, hydroxypropylmethylcellulose; LC–MS/MS, liquid chromatography–tandem mass spectrometry; LM, liver microsome; cNMP, cyclic nucleotide monophosphate; PCP, phencyclidine; PD, pharmacodynamic; PDE, phosphodiesterase; RO, receptor occupancy; SOC, standard of care

## ■ REFERENCES

- (1) Menniti, F. S.; Faraci, W. S.; Schmidt, C. J. Phosphodiesterases in the CNS: targets for drug development. *Nat. Rev. Drug Discovery* **2006**, *5*, 660–670.
- (2) Hebb, A. L. O.; Robertson, H. A. Role of phosphodiesterases in neurological and psychiatric disease. *Curr. Opin. Pharmacol.* **2007**, *7*, 86–92.
- (3) Halene, T. B.; Siegel, S. J. PDE Inhibitors in psychiatry: future options for dementia, depression, and schizophrenia? *Drug Discovery Today* **2007**, *12*, 870–878.
- (4) Miyamoto, S.; Duncan, G. E.; Marx, C. E.; Liberman, J. A. Treatments for schizophrenia: a critical review of pharmacology and mechanisms of action of antipsychotic drugs. *Mol. Psychiatry* **2006**, *10*, 79–104.
- (5) Menniti, F. S.; Chappie, T. A.; Humphrey, J. M.; Schmidt, C. J. Phosphodiesterase 10A inhibitors: a novel approach to the treatment of the symptoms of schizophrenia. *Curr. Opin. Invest. Drugs* **2007**, *8*, 54–59.
- (6) Siuciak, J. A.; McCarthy, S. A.; Chapin, D. S.; Fujiwara, R. A.; James, L. C.; Williams, R. D.; Stock, J. L.; McNeish, J. D.; Strick, C. A.; Menniti, F. S.; Schmidt, C. J. Genetic deletion of the striatum-enriched phosphodiester PDE10A: evidence for altered striatal function. *Neuropharmacology* **2006**, *51*, 374–385.

(7) Kehler, J.; Nielsen, J. PDE10A inhibitors: novel therapeutic drugs for schizophrenia. *Curr. Pharm. Des.* **2011**, *17*, 137–150.

(8) As of the preparation of this manuscript, clinicaltrials.gov reported that two PDE10A inhibitors, PF-02545920 and RO5545965, have entered into clinical trials.

(9) Hu, E.; Kunz, R. K.; Chen, N.; Rumpfelt, S.; Siegmund, A.; Andrews, K.; Chmait, S.; Zhao, S.; Davis, C.; Chen, H.; Lester-Zeiner, D.; Ma, J.; Biorn, C.; Shi, J.; Porter, A.; Treanor, J.; Allen, J. R. Design, optimization, and biological evaluation of novel ketobenzimidazoles as potent and selective inhibitors of phosphodiesterase 10A (PDE10A). *J. Med. Chem.* **2013**, *56*, 8781–8792.

(10) Thomas, V. H.; Bhattachar, S.; Hitchingham, L.; Zocharski, P.; Naath, M.; Surendran, N.; Stoner, C. L.; El-Kattan, A. The road map to oral bioavailability: an industrial perspective. *Expert Opin. Drug Metab.* **2006**, *4*, 591–608.

(11) Hu, E.; Ma, J.; Biorn, C.; Lester-Zeiner, D.; Cho, R.; Rumpfelt, S.; Kunz, R. K.; Nixey, T.; Michelsen, K.; Miller, S.; Shi, J.; Wong, J.; Hill Della Puppa, G.; Able, J.; Talreja, S.; Hwang, D.-R.; Hitchcock, S. A.; Porter, A.; Immke, D.; Allen, J. R.; Treanor, J.; Chen, H. Rapid identification of a novel small molecule phosphodiesterase 10A (PDE10A) tracer. *J. Med. Chem.* **2012**, *55*, 4776–4787.